Received: 11 September 2017 | Revised: 14 November 2017 | Accepted: 14 December 2017

DOI: 10.1002/er.3991

RESEARCH ARTICLE

WILEY INTERNATIONAL JOURNAL OF ENERGY RESEARCH

Modeling representative Gen-IV molten fuel reactivity effects in the ZEPHYR fast/thermal coupled ZPRs. Part I—Assembly level

M. Margulis[1,2] | P. Blaise[3] | E. Gilad[2]

[1]DEN/CAD/DER/SPESI/LP2E, CEA, Cadarashe, Saint-Paul-les-Durance 13108, France

[2]The Unit of Nuclear Engineering, Ben-Gurion University of the Negev, Beer-Sheva 84105, Israel

[3]DEN/CAD/DER/SPESI, CEA, Cadarashe, Saint-Paul-les-Durance 13108, France

Correspondence
M. Margulis, The Unit of Nuclear Engineering, Ben-Gurion University of the Negev, Beer-Sheva 84105, Israel.
Email: maratm@post.bgu.ac.il; marat.margulis@cea.fr

E. Gilad, The Unit of Nuclear Engineering, Ben-Gurion University of the Negev, Beer-Sheva 84105, Israel.
Email: gilade@bgu.ac.il

Summary

The comprehension of severe criticality accident is a key issue in Gen-IV neutronics and safety. Within the future zero-power experimental physics reactor (ZEPHYR), to be built in Cadarache in the next decade, innovative approaches to reproduce high temperature partially degraded Gen-IV cores into a critical facility is being investigated. This work presents the first attempt to represent a fuel assembly of sodium-cooled fast reactor severe criticality accident based on surrogate models. One identified way to construct such representative configuration is to use MASURCA plates stockpile (MOX, UOx, Na, U, and Pu metal) in a fast/thermal coupled core to model a stratified molten assembly. The present study is the first step in a more global approach to full core analysis. The approach is based on a nature-inspired metaheuristic algorithm, the particle swarm optimization algorithm, to find relevant ZEPHYR configuration at 20°C that exhibits characteristics of (2000-3000°C) molten MOX assembly in a stratified metal arrangement in a reference sodium-cooled fast reactor core. Thus, the underlying research question of this study is whether it is possible to represent temperature-related reactivity effects occurring at fuel meltdown temperatures in a power reactor as density-related reactivity effects at the operation temperature of a zero-power reactor, and if so, how should it be done? The calculations are based on a Serpent-2 Monte Carlo sensitivity and representativity analysis using the Cadarache's cross sections covariance data (COMAC). The single fuel assembly studies show that it is possible to represent the multiplication factor with a representativity factor greater than 0.98. As for reactivity variations, it is possible to achieve a satisfactory representativity factor of above 0.85 in all the presented cases. The representativity process demonstrates that temperature effects could be translated into density effects with good confidence. A complementary analysis on modified nuclear data covariance matrix demonstrates the importance of selecting consistent and robust uncertainties in the particle swarm optimization algorithm. This work provides insights on the behavior of the representativity scheme in different core states and shades some light on the problem in hand.

KEYWORDS
ASTRID, core meltdown, energy research, nuclear power, particle swarm optimization, representativity, severe accident, ZEPHYR

1 | INTRODUCTION

Severe core accident (SCA) in sodium-cooled fast reactors (SFRs) is strongly coupled to the neutronic characteristics of the core since the core is not loaded in its most reactive configuration. Therefore, any changes in the loaded configuration (relocation of materials such as fuel, sodium/coolant, absorbers, or even structural materials) have the potential to lead to uncontrolled power excursion. The study of SCA progression requires detailed estimation of the core's neutronic characteristics during the different stages of the SCA. Core reactivity variations could result from many different reasons, where the main contributors are the following[1-3]:

1. Loss of coolant - leads to neutron spectrum hardening and increase in the neutron leakage (usually a negative reactivity effect).
2. Structural material redistribution - could lead to variation in streaming effects and change the direct and adjoint fluxes (could be a positive effect by increasing scattering to high importance regions).
3. Accumulation of molten fuel in certain regions of the core - could potentially alter the high importance region location and lead to reactivity excursion.

The current operating nuclear power plant fleet is heavily based on thermal light water reactors (LWRs), also known as generation (GEN) I to III/III+ reactors. Unlike their future replacements, the GEN-IV reactors, the GEN-I-III/III+ reactors are loaded in their most critical configuration. Therefore, each modification to the core layout is most likely to result in negative reactivity variation and contributes to the core shutdown by increasing leakage, decreased neutron moderation, and/or, in case of reflooding of the voided zone, increase in hydrogen capture in the water. Thus, the study of SCA in GEN-I-III/III+ reactors is mainly focused on the thermal-hydraulic and mechanic properties (eg, steam explosions, hydrogen generation, and oxidation of materials) of the systems,[4] while much less emphasizing the neutronic modeling.

The scenarios mentioned earlier, for SFRs, have the potential to lead to significant alteration in the core neutronic characteristics, which could greatly affect the normal and emergency operation of the reactor. Therefore, support of experimental programs for the analytic research of the core behavior during SCA is imperative for the development of best estimate computational tools. Where the range of possible scenarios of SCA and associated degraded geometries are rather large, and requires a quasi-analytic approach, at least to validate instantaneous critical situations during the meltdown sequence. This last point could be achieved by comparing calculations made by those tools to experimental data available from critical facilities. Ensuring that the experimental program provides meaningful information about the investigated power system (thermal or fast) requires the design of "best representative" configurations. The relation between the power system and the zero-power facility is a major concern for the R&D institutions.[5-7] Best representative experiments provide measurements, according to the end user request, of various significant quantities (eg, reactivity and flux distribution) with respect to the reference system, which can then be translated to the reference system itself.

With the development of the French ASTRID SFR industrial demonstrator, the low void fraction (Coeur à Faible effet de Vide sodium or CFV) core design presents particularities that potentially deserve an experimental validation, in terms of core physics.[8] In the current study, several accidental scenarios are investigated in the CFV design context, in particular, separated degradation of the upper and lower fissile regions, followed by fuel crossing the fertile zone to form a large fissile molten pool. Large uncertainties on the behavior of the fuel could lead to local power excursions. These phenomena can be experimentally modeled in zero-power reactors (ZPRs), such as MASURCA fast critical facility (to start again in 2021 after an important refurbishment phase), or in the future zero-power experimental physics reactor (ZEPHYR) facility[9] (to be built at CEA Cadarache site around 2028).

The CEA Cadarache site provides a unique opportunity in terms of available fuel stockpile at the MASURCA facility (rodlets and plates) of various types of fuel (MOX, UOX, metallic plutonium, and uranium) and other materials available in fast systems (eg, sodium, steel, lead, and graphite) to ensure high representativity of SCA modeling. However, as SCA occurs at high temperature and the experimental facility (ZPR) is operating at room conditions, the representativity process must include the temperature effects in the design process. Therefore, an innovative methodology must be developed to ensure

proper representativity between the hypothetical case and the critical facility.

This paper summarizes the results of the first feasibility studies made on an SCA occurring at the assembly level in the ASTRID and its implementation in the ZEPHYR reactor. The proposed methodology presented in this paper is designed specifically to deal with the representativity of temperature-related reactivity effects at high temperatures during SCA in the reference CFV core by density-related reactivity effects at 20°C in the ZEPHYR experimental core. The paper presents the first results of reactivity effect representativity in ZEPHYR for 2 SCA stages in the ASTRID reactor at 3 different molten fuel temperatures (1000°C, 2000°C, and 3000°C), whereas the reference configuration fuel is at nominal operation temperature (around 900°C). Furthermore, as the representativity process relies on nuclear data (ND) uncertainties, some feedback on uncertainties role in the design process is presented as well.

The study presented in this paper is a result of collaboration between CEA Cadarache and Ben-Gurion University of the Negev. The study is a first of a kind feasibility study made in the framework of the ZEPHYR project for SCA investigation.

1.1 | The ZEPHYR project

Post-Fukushima[10] requirements of the French regulatory authorities imply that 2 major French ZPRs, EOLE, and MINERVE will definitively end their operation by the end of 2017. This lead CEA to invest in an innovative facility called ZEPHYR, which would provide support that was given by the 2 old facilities to the needs of the industry and research for the next 5 decades. For the last decades, the MINERVE ZPR located in Cadarache has produced a large range of experimental data in support of ND improvement, mainly for LWRs but also for the fast spectrum reactors through the PHENIX and Super PHENIX projects, while EOLE produced a unique database for the development and the integral validation of advanced LWR calculation schemes and associated ND libraries in representative mock-ups.

In parallel with R&D studies on SFRs, in particular, the ASTRID technological demonstrator, a new interest for fast-thermal coupled cores already investigated in the 70s[11] rose up. Those configurations consist of getting fast-spectrum neutronics characteristics in a reduced central zone, also called the "measurement zone" or "experimental zone" while criticality is achieved using a thermal driver zone. As this latter gathers most fission, such configurations allow an important reduction of fissile materials and a higher flexibility due to the thermal spectrum kinetics parameters. The main issue is then to provide a proper fast spectrum in the center by using an adapted spectral conversion zone, surrounded by the thermal spectrum zone. This work has been extensively revisited —major coupled cores design characteristics and conclusions can be found in Ros et al.[12] Hence, within the new awaited innovative feature of the ZEPHYR project, coupled core physics is one of the most promising outcomes for performing neutron physics and improve both codes and ND.

Figure 1 presents the proposed coupled configuration for the ZEPHYR core. The thermal part of a fast/thermal coupled core can work in either booster or coupling region and can then amplify local effects in the fast zone, suitable, for example, for ND improvement. Another particularity of fast/thermal is the improvement of the spectrum and reactivity effects representativity in the fast zone against infinite lattice fast cells, hence reducing the number of fuel materials while guaranteeing the correct neutron spectrum on a large area.[9]

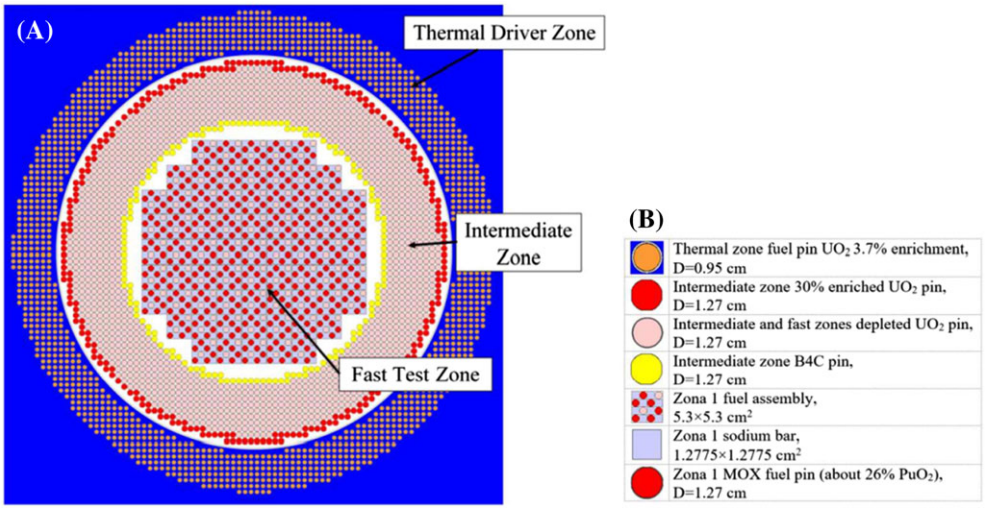

FIGURE 1 Proposed ZEPHYR core layout. A, Core layout. B, Pin description [Colour figure can be viewed at wileyonlinelibrary.com]

2 | METHODOLOGY

In this section, the proposed methodology for the SCA experimental program design is presented. The mathematical model of the representativity process is summarized, as well as the utilization of this model in the representative configuration design optimization.

2.1 | Representativity estimation

Experimental programs in critical facilities or ZPRs play a key role in the validation of neutron lattice and core codes as they enable the access to information neither reachable in power reactors nor existing new concepts. Numerical methods and the accuracy of calculated parameters are constantly improving. This improvement, in addition to the utilization of high-performance computing, requires new approaches to the design of experimental programs compared to the past design studies. One proposed approach uses the representativity concept[13] to enhance the information transfer from the mock-up to the actual reactor design (eg, nondimensional analysis).

As mentioned previously, the importance of best representative experimental design is a key factor in the safe design of future nuclear systems. By ensuring representation of a large number of integral parameters, one can provide a "best estimate" for the investigated system in a controlled environment of a ZPR. In cases, for which the experimental mock-up resembles the reference system and similar quantities are considered in the 2 systems, only minor corrections are generally necessary. However, if the 2 systems differ to some extent (eg, the fuel type or enrichment), although the useful information contained in the measurements remains significant, full use of the experimental results can become a problem.

The representativity method[13] is used to quantify the relationship between the particular integral response of an experimental mock-up and the same response in an examined (power) system that is under investigation. The base of the method is the similarity comparison of the sensitivity profile of the same integral quantity. The representativity is linked to the definition of a correlation coefficient (noted as r_{RE}) and defined by Equation 1.[13]

$$r_{RE} = \frac{\boldsymbol{S}_{\boldsymbol{R}}^{\boldsymbol{t}} \cdot \boldsymbol{V} \cdot \boldsymbol{S}_{\boldsymbol{E}}}{\sqrt{\boldsymbol{S}_{\boldsymbol{R}}^{\boldsymbol{t}} \cdot \boldsymbol{V} \cdot \boldsymbol{S}_{\boldsymbol{R}}} \cdot \sqrt{\boldsymbol{S}_{\boldsymbol{E}}^{\boldsymbol{t}} \cdot \boldsymbol{V} \cdot \boldsymbol{S}_{\boldsymbol{E}}}} \quad (1)$$

where the subscripts $\boldsymbol{E}$ and $\boldsymbol{R}$ correspond to the experimental mock-up and reference power systems, respectively; $\boldsymbol{S}$ is the sensitivity vector of the integral quantity to ND in the 2 systems; $\boldsymbol{V}$ is the variance-covariance matrix between ND; and $\boldsymbol{S}_{\boldsymbol{E}}^{\boldsymbol{t}} \cdot \boldsymbol{V} \cdot \boldsymbol{S}_{\boldsymbol{E}}$ and $\boldsymbol{S}_{\boldsymbol{R}}^{\boldsymbol{t}} \cdot \boldsymbol{V} \cdot \boldsymbol{S}_{\boldsymbol{R}}$ represent, respectively, the priori variance $\boldsymbol{E}$ and $\boldsymbol{R}$ due to ND uncertainties, propagated by the classical "sandwich" rule.[14]

The numerator in Equation 1 represents the covariance between the experiment and the reactor response formally, while the denominator is simply the square-rooted product of the variance of $\boldsymbol{E}$ and $\boldsymbol{R}$. The larger the magnitude of r_{RE}, the higher the information transferred from the mock-up test to the target systems designs. When the similarity of $\boldsymbol{S}_{\boldsymbol{E}}$ and $\boldsymbol{S}_{\boldsymbol{R}}$ increases, the value of the representativity factor r_{RE} reaches an optimum value of unity, which indicates fully correlated neutron systems, with respect to the variance-covariance matrix used.

The representativity approach also enables to predict a posteriori reduction in the reactor response uncertainty, ϵ_R^*, after having injected the experimental information into a complete Bayesian assimilation process ("adjustment") of multigroup cross sections. The reduction factor is given by the expression in Equation 2.[13]

$$\begin{aligned}\left(\epsilon_R^*\right)^2 &= (\epsilon_R)^2 \cdot \left(1 - \frac{r_{RE}^2}{1 + \delta E^2 / \left(\boldsymbol{S}_{\boldsymbol{E}}^{\boldsymbol{t}} \cdot \boldsymbol{V} \cdot \boldsymbol{S}_{\boldsymbol{E}}\right)}\right) \\ &= (\epsilon_R)^2 \cdot \left(1 - \frac{r_{RE}^2}{1 + \delta E^2 / \epsilon_E^2}\right) = (\epsilon_R)^2 \cdot \left(1 - \omega r_{RE}^2\right), \quad (2)\end{aligned}$$

where δE^2 is the experimental uncertainty on the response E, ϵ_R is the priori reduction in the reactor response uncertainty, and $\omega = \left(1 + \delta E^2 / \epsilon_E^2\right)^{-1}$ is what can be called the "experimental weight" factor or the "experimental importance," which represents the amount of transferable precision (ie, experimental uncertainty) of the integral parameter versus the propagated uncertainty from ND. In the limit of $r_{RE} = 1$ and the ratio $\delta E^2 / \epsilon_E^2 \to 0$, the reduction factor, $\epsilon_R^* / \epsilon_R$, can vanish.

As mentioned earlier in the text, the goal is to achieve a highly representative experimental configuration with the highest possible value of r_{RE} (unity). However, for reactivity variation with little variation in the material loading in the core, the sensitivity vector values are quite low and strongly affected by any variation in the core, as learned from previous experiments analysis.[15,16] Therefore, the minimal accepted representativity factor for this project is set to $r_{RE} = 0.85$. The remaining open question is how to achieve that goal, given the large number of parameters influencing the problem (ie, material, geometry, and temperature). The proposed solution for achieving the desired representativity factor is discussed in the following section, along with the utilized tools and assumptions made.

2.2 | Design optimization process

Ultimately, the methodology is based on the use of MASURCA stockpile in ZEPHYR assemblies to reproduce stratified SFR degraded assemblies. Thanks to the unique available stockpile in MASURCA (Figure 2), a proper selection of adequate MOX, UOx, SS, and Na materials can be used:

1. Rodlets for undegraded assemblies.
2. Platelets for degraded (melted) parts of assemblies.

However, as this is a preliminary study, only the best possible solution is considered. The design optimization process must integrate the temperature effect. Indeed, the aim is to reproduce consistent reactivity effects from the SFR target at hot full power (HFP) to ZEPHYR at 20°C. A classical approach based on geometrical representativity as a first guess can induce strong bias in the result. The following strategy is then developed:

- STEP I—Calculate the known SFR reference configuration and associated ND-based sensitivity profiles at HFP temperature.
- STEP II—First optimization step, to determine the most representative configuration at 20°C, by adjusting the PuO_2 concentration in the MOX, to be loaded into the ZEPHYR to ensure best representativity of the previous step.
- STEP III—Calculate the known SFR degraded configurations and their associated ND-based sensitivity profiles at 1000°C, 2000°C, and 3000°C temperatures.
- STEP IV—Second optimization step, to determine the optimal amount of PuO_2 in the MOX fuel that ensures the best representative reactivity variation between the reference SFR calculated in Steps I and III, and the ZEPHYR configuration from Step II.
- STEP V—Ultimately, select fuel plates available in the MASURCA stockpile to correspond as closely as possible to the found parameters in Step IV.
- STEP VI—Finally, recompute the realistic representativity, based on the currently available stockpile.

The search space of the different parameters, such as geometry and material content, is huge, and it is practically impossible to scan it deterministically. Therefore, to explore efficiently the search space for the best possible solutions, an optimization algorithm based on the particle swarm optimization (PSO)[17] has been selected as an efficient optimization approach.

The PSO is a swarm intelligence metaheuristic, which was inspired by the flocking behavior of animals (ie, flock of birds and group of fish). Similarly, to the genetic algorithm (GA), the PSO is a population-based method, which is used to represent the state of possible problem solution by its population. The population of the PSO is iterated through generations until some termination criterion is satisfied. The population, $P = \{p_k\}_{k=1}^{n}$, which is often called the swarm, consists of n single feasible solutions (p_k) also known as particles, which are located inside the search space.

In the current study, the particles of the PSO are subjected to predefined constraints (ie, content of PuO_2 in the MOX fuel or specific zone geometrical parameters) and are iterated by executing the Monte Carlo base code Serpent 2 with extended capabilities for obtaining the sensitivity profiles,[18] followed by evaluation of the representativity factor for the current particle. After the evaluation of the representativity factor, the particle is updated with respect to 2 key factors: the particle self-best result and the entire swarm best location. The algorithm of the PSO is summarized in Algorithm 1. Appendix 1 provides general overview and terminology of the PSO algorithm.

As mentioned previously, the evolution of the position of each particle between iteration requires an update process. In the PSO algorithm, the update process is done through the estimation of the particle velocity with

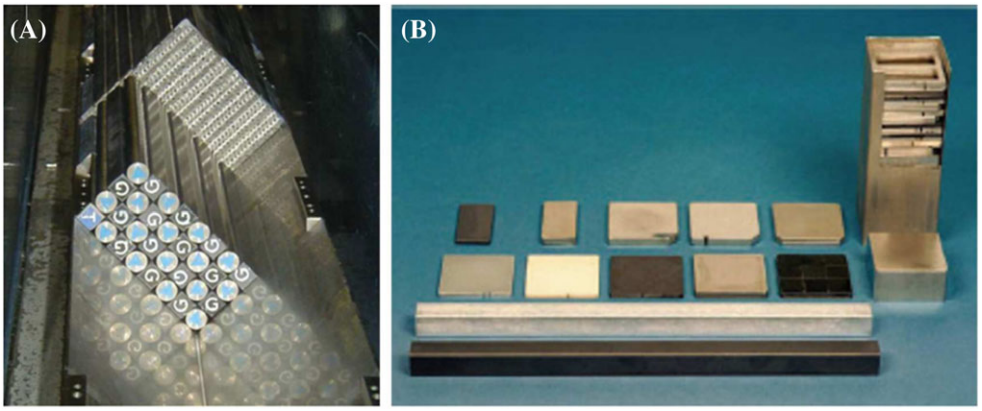

FIGURE 2 MASURCA reactor available stockpile. A, Pins. B, Plates [Colour figure can be viewed at wileyonlinelibrary.com]

respect to both the particle and the entire swarm best-known locations. The calculation of the velocity and the update of the particle position are done according to Equations 3 and 4, respectively.

$$v_i^{k+1} = \chi \cdot \left[\omega \cdot v_i^k + c_1 \cdot \mathrm{rand}_1 \cdot (pop.best_i - pop.cost_i) + c_2 \cdot \mathrm{rand}_2 \cdot (global.best - pop.cost_i)\right] \quad (3)$$

$$pop.pos_i^{k+1} = v_i^{k+1} + pop.pos_i^k, \quad (4)$$

where the indices k and i stand for iteration and particle in the population, respectively; χ is the so-called constriction factor, which is used to improve convergence (in this study, χ is set to unity); ω is the personal inertia weight parameter and is iteration dependent, as given in Equation 5a; c_1 and c_2 are the *cognitive* and *social* coefficients, respectively, calculated according to Equation 5b and 5c, respectively; $rand_1$ and $rand_2$ are random numbers between 0 and 1; $pop.\ cost_i$ is the current estimation of particle i; $pop.\ best_i$ is the best estimation of particle i; and *global. best* is the best estimation of the entire swarm.

$$\omega = \omega_{min} + (\omega_{max} - \omega_{min}) \cdot \frac{iter_{max} - iter}{iter_{max}}, \quad (\omega_{max} = 0.9\, and\, \omega_{min} = 0.4) \quad (5a)$$

$$c_1 = c_{1i} + (c_{1f} - c_{1i}) \cdot \frac{iter}{iter_{max}}, \quad (c_{1i} = 2.5\ and\ c_{1f} = 0.5) \quad (5b)$$

$$c_2 = c_{2i} + (c_{2f} - c_{2i}) \cdot \frac{iter}{iter_{max}}, \quad (c_{2i} = 0.5\ and\ c_{2f} = 2.5) \quad (5c)$$

Algorithm 1. PSO algorithm

```
Procedure PSO-R(n,constraints,maxIt)
  pop.pos = Generate random pop(n,constraints)
  pop.cost = Evaluation representativity for each particle (Serpent)
  pop.best = Update personal bests
  global.best = Update global bests
  while i < maxIt do
    pop.v = Update velocity of each particle
    pop.pos = pop.pos + pop.v, Update position of each particle
    pop.cost = Evaluate representativity for each particle (Serpent)
    pop.best = Update personal bests
    global.bests = Update global bests
  end while
  Return Best Particle
end procedure
```

In classical PSO, the definition of the cognitive (c_1) and the social (c_2) coefficients are set to a constant (the value commonly used is 2.1 for both coefficients[17]). However, as in many optimization algorithms, a chance exists of converging to a local and not a global minimum. Therefore, to overcome this problem, it is proposed to introduce evolution to the 2 coefficients, as presented in Equations 5b and 5c.[19] As can be seen, the importance of the cognitive coefficient at the first iterations is much higher, which allows the particle to explore its environment. On the other hand, as the iterative process continues, the importance of the cognitive coefficient is reduced, and the social impact on the particle velocity grows, which pulls the particles towards the global best location. This methodology allows for better search and convergence in huge search spaces.

2.3 | Variance-covariance data

As can be seen from Equation 1, the representativity factor estimation is strongly dependent on the variance-covariance matrix ($\boldsymbol{V}$). In this study, all the calculations are performed with the JEFF-3.1.1 ND evaluation, and the variance-covariance data associated with this evaluation in the covariance matrices Cadarache (COMAC) version 01.[20] In the COMAC-V01, some of the key isotopes (especially ^{238}U and ^{239}Pu) are associated with high uncertainties on the key reactions, as shown in Figure 4. However, as the ND evaluation is a dynamic field, new evaluations with new covariance data will become available in the near future (eg, JEFF-3.2 evaluation[21]), together with reduced uncertainties.

Therefore, there is a need to examine the impact of reduced uncertainties on the representativity process. As a first attempt to point out the impact of ND covariance on the PSO representativity process, an *adjusted* set of covariance, denoted hereafter UCOM-V01AB (updated covariance matrix), is also used for comparison.

The UCOM-V01AB is an adjusted version of the COMAC-V01 version using an experimental data available from the recently published SNEAK-12A/B benchmark,[15,16,22,23] which focused on severe accident in liquid metal–cooled fast reactors. The results of the benchmark calculation based on the JEFF-3.1.1 library with the Serpent 2 code show excellent agreement. Therefore, those experiments (while not dedicated to ND feedback) were selected to be included in a ND assimilation tendency investigation. The re-assimilation of the JEFF-3.1.1 library led to no significant deviation before and after the assimilation. However, the covariance data were noticeably impacted, as can be seen from Figures 3 and 4 for ^{238}U and ^{239}Pu capture cross section for COMAC-V01 and UCOM-V01AB, respectively. It should be noted that

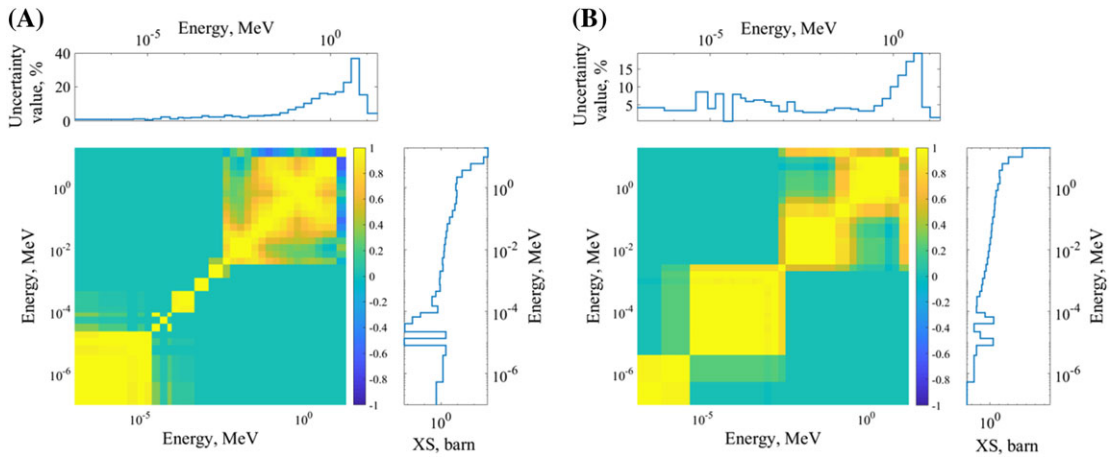

FIGURE 3 Associated uncertainties for capture reaction available in COMAC-V01. A, ^{238}U. B, ^{239}Pu [Colour figure can be viewed at wileyonlinelibrary.com]

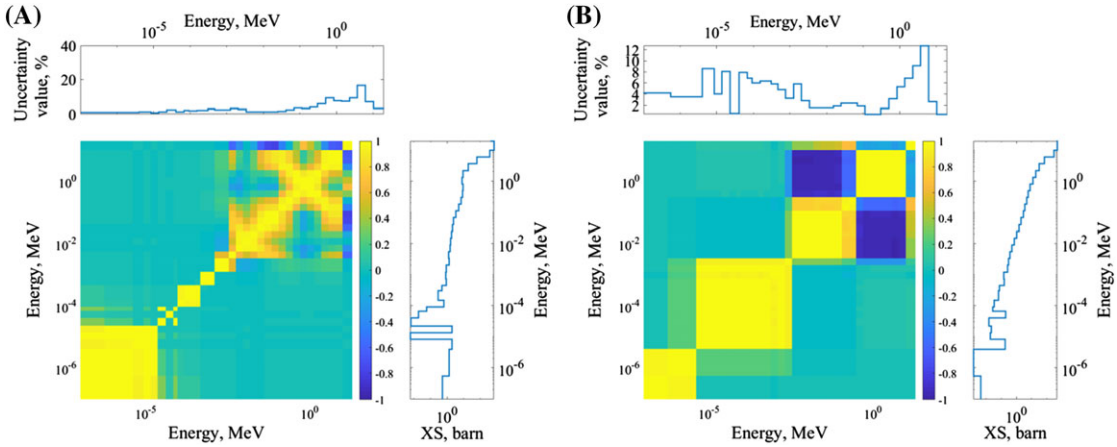

FIGURE 4 Associated uncertainties for capture reaction available in UCOM-V01AB. A, ^{238}U. B, ^{239}Pu [Colour figure can be viewed at wileyonlinelibrary.com]

this covariance matrix is an adjusted one and is thus not associated with any official ND library. However, even if it has been created for internal purpose only, it allows to point out possible effects of important modifications in major isotopes on the representativity results.

As mentioned previously, this SCA study is focused on the ASTRID-CFV core, which is described in detail in Section 3. To clearly understand the impact of the different covariance matrices have on the propagated uncertainties, an isotopic/reaction propagated uncertainties breakdown is calculated and summarized in Figure 5. The results indicate a significant difference for the 2 largest contributors to the total propagated uncertainty (^{238}U and ^{239}Pu), with some additional minor changes in the other plutonium isotopes and the non-fissile/fertile materials. The total propagated uncertainty drops from about 1350 pcm with COMAC-V01 to about 650 pcm with UCOM-V01AB. Therefore, the impact of the covariance data with reduced uncertainties on the representativity process must be examined, as it might change significantly the obtained results from the optimization process.

3 | EXAMINED CONFIGURATIONS

The ASTRID reactor is designed to answer all the requirements for safety, sustainability, economy, and nonproliferation set by the GEN-IV forum.[24] In recent years, several concepts of the ASTRID core were examined.[25] In this study, the selected reference system is based on the ASTRID CFV-V0 core configuration, with several accidental scenarios already investigated.[8] The main characteristics of the CFV-V0 core are summarized in Table 1 and shown in Figure 6, and the approximate plutonium vector of the ASTRID core is summarized in Table 2.[26,27]

Severe core accident, in general, is a noncoherent stepwise process and could develop in various directions. In the case of the ASTRID CFV core, several SCA requires

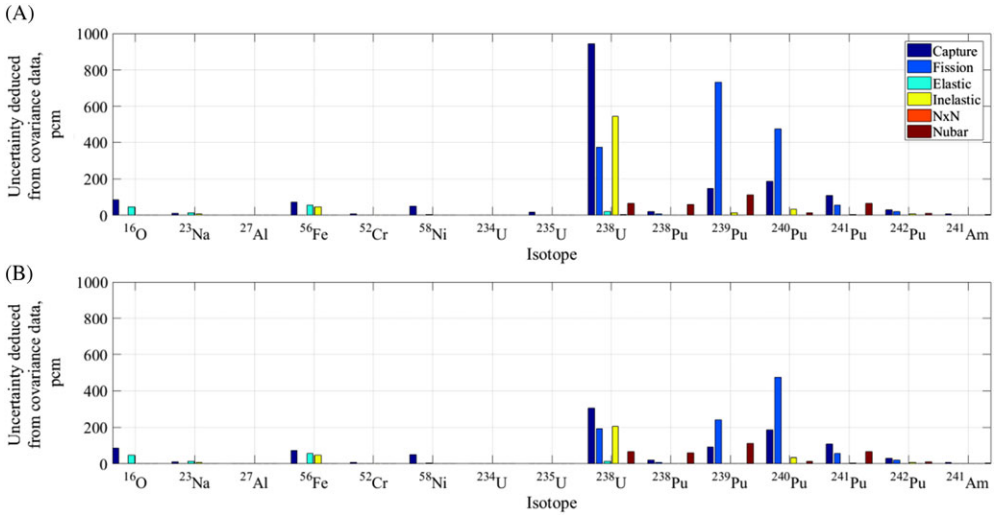

FIGURE 5 Propagated uncertainties for the ASTRID-CFV core isotope/reaction break down obtained with different covariance matrices. A, COMAC-V01. B, UCOM-V01AB [Colour figure can be viewed at wileyonlinelibrary.com]

TABLE 1 Design parameters for the CFV-V0 core[8]

Core Design Parameter	CFV-V0
Nominal thermal power, MW	1500
Inner fissile zone height, cm	25/35
Outer fissile zine height, cm	100
Inner fertile zone height, cm	20
Inner zone radius, cm	133.5
Outer zone radius, cm	162.6
Sub-assembly pitch, cm	17.5
Fissile zone PuO_2 enrichment (inner/outer), % vol	22.8/22.8
Effective delayed neutron fraction (β_{eff}), pcm	364
Void effective reactivity effects ($) core at equilibrium	−1.2

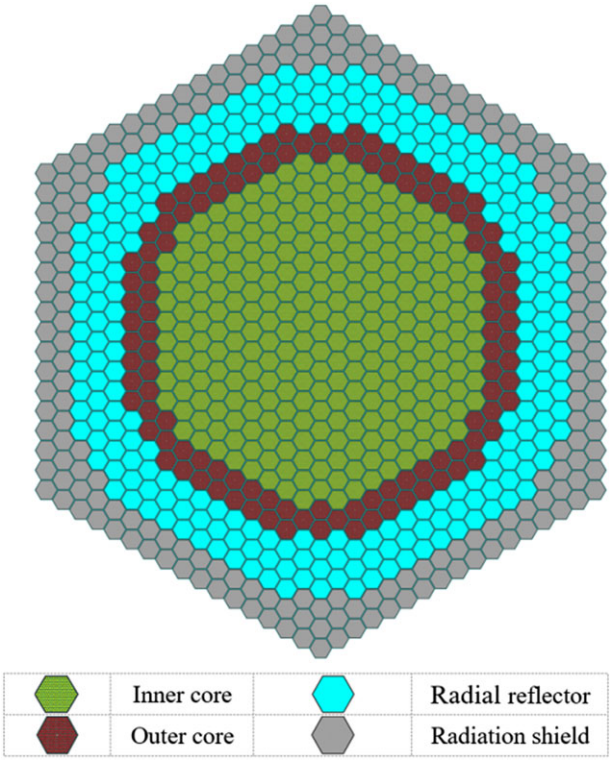

FIGURE 6 ASTRID-CFV-V0 core layout [Colour figure can be viewed at wileyonlinelibrary.com]

investigation due to the heterogeneous axial arrangement of the fuel assembly, as shown in Figure 7A. It should be noted that in this study, the leading initiator of the SCA is a total instantaneous blockage of a single fuel assembly. Therefore, the effect of the sodium in the upper plenum is neglected, simplifying a bit the representativity process. This assumption eliminates the reflection of neutrons from the sodium plenum down to the active core region in case of an accident. Under this assumption, it is possible to consider only the inner axial fissile and fertile zones of the ASTRID core, which make about 110 cm. When assuming sodium in the upper plenums, the height of the examined fuel assembly can reach 200 to 250 cm. This assumption is made due to the fact that the fixed height for a fuel assembly to be loaded into the ZEPHYR is about 90 cm, which could lead to the problem of the fuel assembly scaling and could not represent the leakage of the ASTRID configuration properly.

The first axial cut-off configuration under investigation is reproduced in Figure 7B. It is assumed that both fissile regions underwent a meltdown with stratification of the structural materials depending on the density—

the heavy metal is dropping down, as the structural materials (mainly stainless steel, as well as oxides) remain in the upper part of the fissile zone. The fertile intermediate zone is not impacted by the fuel relocation. The second investigated configuration is reproduced in Figure 7C. In this case, the 2 fissile zones and the separating fertile zone are mixed together. A stratification of the materials depending on the densities is also taken into account—The structural materials are located above the formed molten fuel region. All simulations consider the absence of sodium in the assembly.

The main goal of this study is to find the most representative configurations to ensure the best representativity factor of the reactivity variation between them. However, to ensure a deeper level of representativity (eg, both multiplication factor and reactivity variation), the representativity process is executed in 2 steps, as mentioned earlier. First, determine the most representative configuration of ZEPHYR assembly of the reference ASTRID fuel assembly (Figure 7A). Thus, the ZEPHYR first configuration, in the current work, is representative of the multiplication factor of the ASTRID assembly. Second, the degraded ZEPHYR assembly configuration is searched through the representation of the reactivity variation between the 2 ASTRID configurations and the fixed already in the first step representative configuration of the ZEPHYR. In terms of the multiplication factor, both ZEPHYR configurations are highly representative of the 2 ASTRID configurations, reference and degraded, which is an inherited characteristic of the presented optimization process. This process results are summarized in the following section.

TABLE 2 Approximate plutonium vector of the CFV-V0 core[26,27]

^{238}Pu	^{239}Pu	^{240}Pu	^{241}Pu	^{242}Pu	^{241}Am
3%	55%	26%	7%	7.5%	1.5%

4 | RESULTS AND DISCUSSION

This section deals with the first tests of the optimization approach on the assembly level only. Although the information obtained in this section requires validation on the core level, the results provide insight on the main governing phenomena in the 2 systems, ie, mainly how the *temperature effects* can be translated into *density effects*. These 2 effects are the main focus of the current study, in addition to the examination of the search space (in the case of this work, the content of PuO_2 in the different MOX fuel regions). It should be noted that the Pu vectors are not modified in the optimization process and regarded as a constant in both systems. In the case of the ZEPHYR, the Pu vector is defined according to the available plates in the MASURCA stockpile.

This section is constructed as follows: First, the physics (sensitivity/uncertainty) of the ASTRID reference fuel assembly (Figure 7A), with the governing isotopes identification, is presented. Second, a sensitivity/uncertainty analysis on the reactivity variation between the different ASTRID degraded configuration using Serpent capabilities is performed. Third, the results of the PSO are described for the different configurations, taking the temperature effects between the 3 ASTRID cases and the ZEPHYR targets into consideration. An additional paragraph is devoted to the impact of the variance-covariance

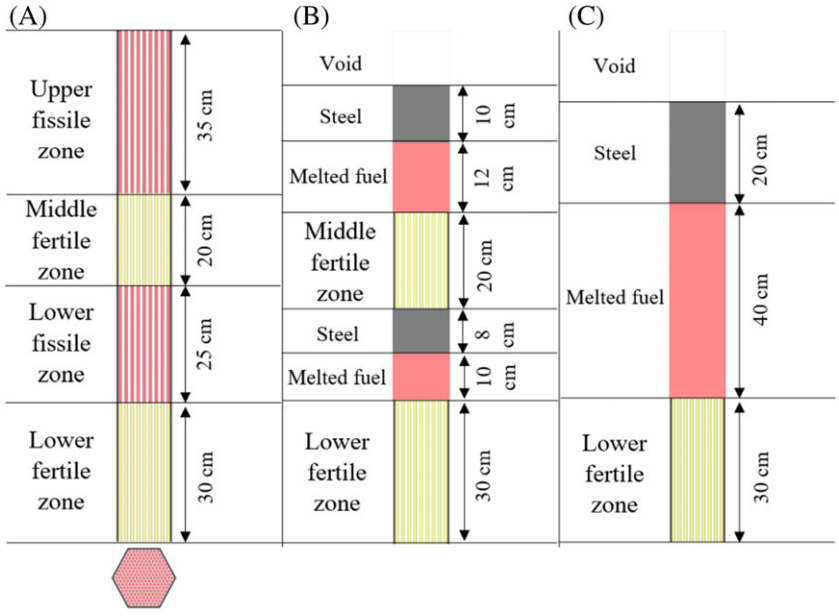

FIGURE 7 ASTRID severe core accident sequences under investigation. A, Voided reference configuration. B, 2-zone degraded configuration. C, Single degraded configuration [Colour figure can be viewed at wileyonlinelibrary.com]

data. Finally, the behavior of the most representative configuration is discussed in comparison to the ASTRID configuration.

4.1 | Identification of problem driving parameters

Detailed interpretation of similar programs[15,16] showed that in case the change in the material balance between different SCA configurations is not large, the sensitivity vector and the propagated uncertainties remain quite similar. Therefore, to determine the largest contributors to the total propagated uncertainty on the multiplication factor, the examination of the reference configuration should suffice. Hence, 2 clear configurations are examined: For the first configuration, the entire system is set at 20°C, whereas for the second configuration the system is set at 600°C and the fuel at 900°C. This latest situation corresponds to HFP conditions. Indeed, 20°C is not a realistic situation, as sodium might be present in a solid state at this temperature. Thus, this temperature is taken just as a theoretical reference for the current study. The analysis identified the following isotopes as the most significant to the problem: ^{16}O, ^{56}Fe, ^{238}U, and ^{238,239,240,241}Pu. The propagated uncertainties for those isotopes are summarized in Figure 8.

Generally, the 2 analyses yield similar propagated uncertainties. However, there are some notable differences, with a general trend visible in a reduction in all the capture propagated uncertainties and increase in the other reactions. Notable changes are given in Table 3. This is mainly due to the hardening of the spectrum (at 900°C), as shown in Figure 9, which leads to changes in the sensitivity vectors. The main visible effect in the propagated uncertainties is visible in the ^{238}U (Figure 8). The temperature change causes a reduction in the sensitivity coefficients of capture and increase in fission and inelastic scattering, as can be seen in Figure 10.

Through this work, the presentation of the sensitivity vectors is made through a "sensitivity comparative

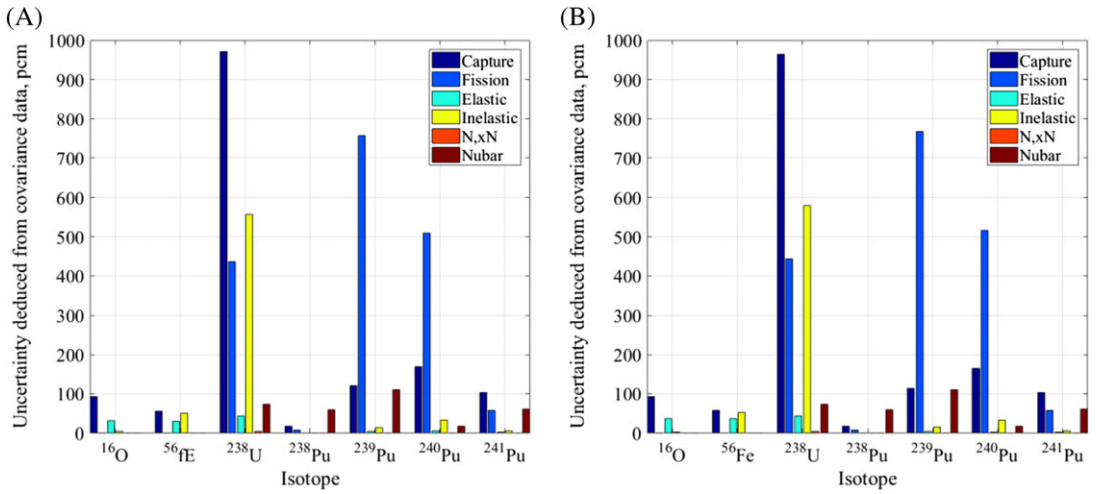

FIGURE 8 Reaction/isotope propagated uncertainty breakdown for 2 reference configurations with COMAC-V01 for ASTRID assembly. A, Fuel at 20°C. B, Fuel at 900°C. The differences between the figures can be observed in detail in Table 3 [Colour figure can be viewed at wileyonlinelibrary.com]

TABLE 3 ASTRID reference configuration: differences in propagated uncertainties values due to temperature variation

Isotope	Reaction	20°C Config., pcm	900°C Config., pcm	Difference, %
^{16}O	Elastic scattering	31	36	14
^{56}Fe	Elastic scattering	30	35	17
^{238}U	Capture	971	960	−1.5
	Fission	436	443	1.6
	Inelastic scattering	550	580	5.5
^{239}Pu	Capture	110	125	−14
	Fission	755	770	2
^{240}Pu	Capture	170	160	−6
	Fission	505	515	2

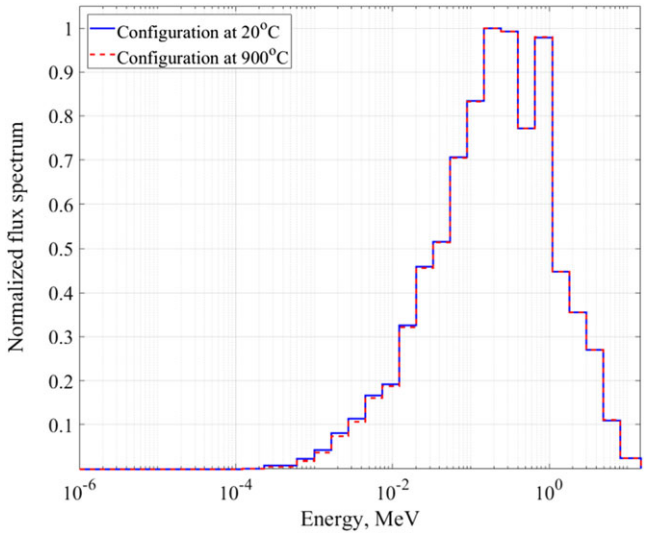

FIGURE 9 Reference configuration normalized flux spectrum as a function of temperature [Colour figure can be viewed at wileyonlinelibrary.com]

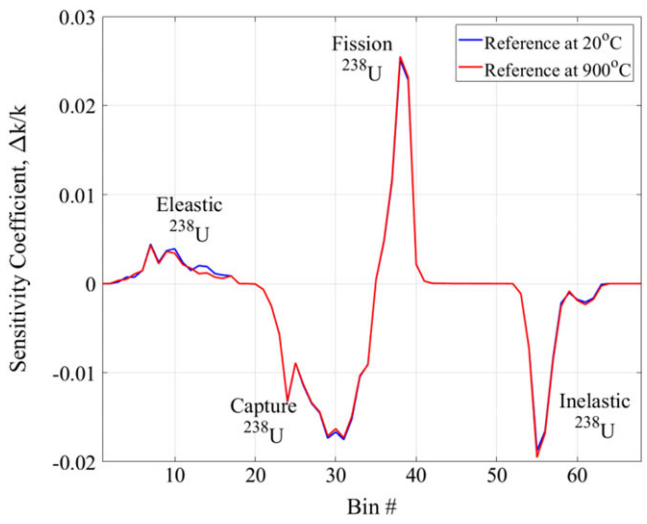

FIGURE 10 Total sensitivity vector of ^{238}U for 2 different ASTRID clear configurations [Colour figure can be viewed at wileyonlinelibrary.com]

visualization," as can be seen, eg, Figure 10. In this type of visualization, there is no consideration of isotope, reaction, or energy in the usual direct form, but rather a continues numeration of all the considered isotopes reactions and energy groups. Thus, *Bin* is a vector of continues numeration from one to the *isotopes* × *reactions* × *energy gropus*. Where *isotope* are ^{238}U, ^{239}Pu and ^{240}Pu, *reactions* are elastic scattering, capture, fission and inelastic scattering, and *energy groups* are the 14 energy groups from 5.5 KeV to 20 MeV according to the typical ECCO 33 energy groups structure.[28]

4.1.1 | A note on the utilization of the reduced uncertainty variance-covariance matrix, UCOM-V01AB

Due to the modification of some major reaction uncertainties, mainly those of ^{238}U and ^{239}Pu (Figures 3 and 4), those important changes in the propagated uncertainties can substantially influence the representativity calculation process. By using COMAC-V01 matrix, the optimization problem is mainly governed by ^{238}U and ^{239}Pu, as seen from Figure 8. By using the UCOM-V01AB in the uncertainty propagation rule, the representativity process becomes more complex as its dependency on the ^{240}Pu increases significantly (Figure 11), hence inducing severe modification of the final PuO_2 quantities in the target ZEPHYR configuration. This problem is presented in detail in the following sections regarding the representativity of the fuel assembly multiplication factor (Section 4.3) and the representativity of the reactivity variation (Section 4.4).

4.2 | ASTRID reactivity variation reference

Previous experiment analysis of similar programs such as SNEAK-12A and 12B pointed out the removal of sodium from the core as the largest impact on the reactivity variation ($\Delta\rho$) sensitivity/uncertainty parameters,[15,16,29] while the geometrical changes have a much lower impact.[16] Furthermore, in the current study, the reactivity variation between the different cases are large (Tables 4 and 5), which in turn substantially reduces both the sensitivity vectors and the propagated uncertainties on $\Delta\rho$. This can be seen from the equation for the sensitivity vector ($\boldsymbol{S}$) of $\Delta\rho$ on reaction μ, Equation 6.

$$\boldsymbol{S}(\Delta\rho,\mu) = \frac{1}{\Delta\rho}\cdot\left(\frac{\boldsymbol{S}(k_2,\mu)}{k_2} - \frac{\boldsymbol{S}(k_1,\mu)}{k_1}\right) \tag{6}$$

Several examples of the flux spectrum, total sensitivity vector for the multiplication factor, and the reactivity variations are given in Figures 12 and 13. The results show that the flux spectrum is slightly more thermal in the degraded configuration in comparison to the reference (as seen from Figures 12A and 13A). The total sensitivity vector of the assembly multiplication factor (Figures 12B and 13B) experience profound changes as a function of the configuration examined. However, as mentioned previously, due to the large reactivity variation between the different configuration, the sensitivity vector of the reactivity variation is very small (Figures 12C and 13C). The last is the reason for the low total propagated uncertainties on the reactivity variation.

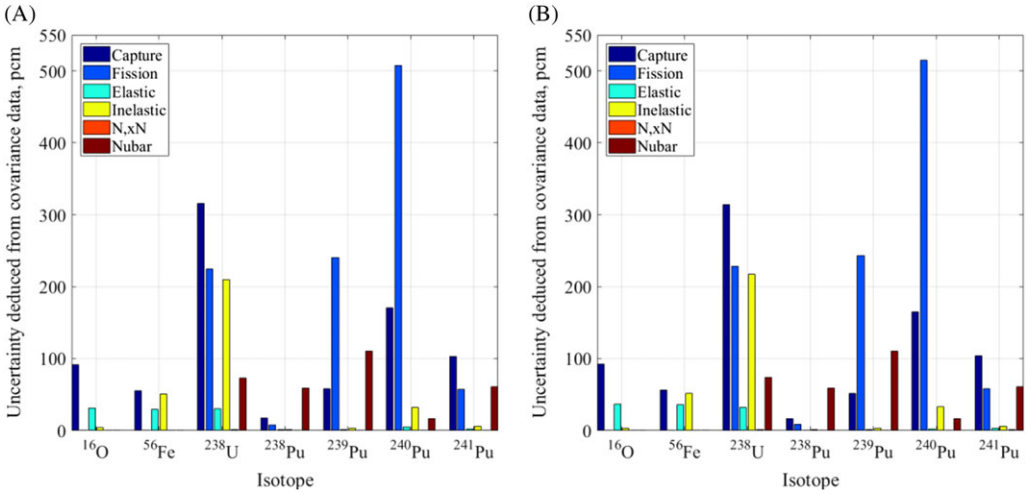

FIGURE 11 Reaction-isotope propagated uncertainty breakdown for 2 ASTRID assembly reference configurations with UCOM-V01AB. A, Fuel at 20°C. B, Fuel at 900°C [Colour figure can be viewed at wileyonlinelibrary.com]

TABLE 4 ASTRID reference configurations' multiplication factors as a function of temperature

Configuration	20°C	900°C	1000°C	2000°C	3000°C
Config. 1—Reference (Figure 7A)	1.13774	1.12871	...	...	...
	±3.7E-05	±3.7E-05	...	...	...
Config. 2—Degraded 1 (Figure 7B)	1.08755	...	1.07823	1.07622	1.07507
	±3.9E-05	...	±4.0E-05	±4.0E-05	±4.0E-05
Config. 1—Degraded 2 (Figure 7C)	1.34957	...	1.33938	1.33682	1.33543
	±3.3E-05	...	±3.3E-05	±3.3E-05	±3.3E-05

TABLE 5 ASTRID reference configurations' reactivity variations as a function of temperature in pcm

Reference	Reference at 20°C	Prop. Unc.	Reference at 900°C	Prop. Unc.
Config. 2—Deg. 1 at 20°C	−4056	4E-02	...	...
Config. 2—Deg. 1 at 1000°C	...	...	−4178	3.7E-02
Config. 2—Deg. 1 at 2000°C	...	...	−4321	3.6E-02
Config. 2—Deg. 1 at 3000°C	...	...	−4420	3.5E-02
Config. 3—Deg. 2 at 20°C	13795	1.6E-02	...	...
Config. 2—Deg. 2 at 1000°C	...	...	13935	1.6E-02
Config. 2—Deg. 2 at 2000°C	...	...	13790	1.7E-02
Config. 2—Deg. 2 at 3000°C	...	...	13710	1.8E-02

One interesting behavior is visible in the sensitivity of the reactivity variation to the changes in the inelastic scattering cross section of ^{238}U, for which the sensitivity changes signs between the 2 different degraded cases reactivity variation sensitivity vectors. This is due to the fact that in the degraded 1 configuration (lines denoted "Ref. vs Deg. 1 at 20°C" in Figure 12C or "Ref. at 900°C vs Deg. 1 at 1000°C" in Figure 13C), as in the degraded 1 configuration there is still 2 fissile zones separated by an undamaged fertile zone, this zone serves as a reflector for the lower degraded zone. Thus, neutrons are scattered back from the fertile zone. On the other hand, in the second reactivity variation case (lines denoted "Ref. vs Deg. 2 at 20°C" in Figure 12C or "Ref. at 900°C vs Deg. 2 at 1000°C" in Figure 13C), inelastic scattering in ^{238}U is reduced and becomes negative, due to the fact that in this configuration, ^{238}U is present in the melted zone, and it contributes to the scattering of neutrons out of the degrade area, which leads to the negative sign on the contribution to the reactivity.

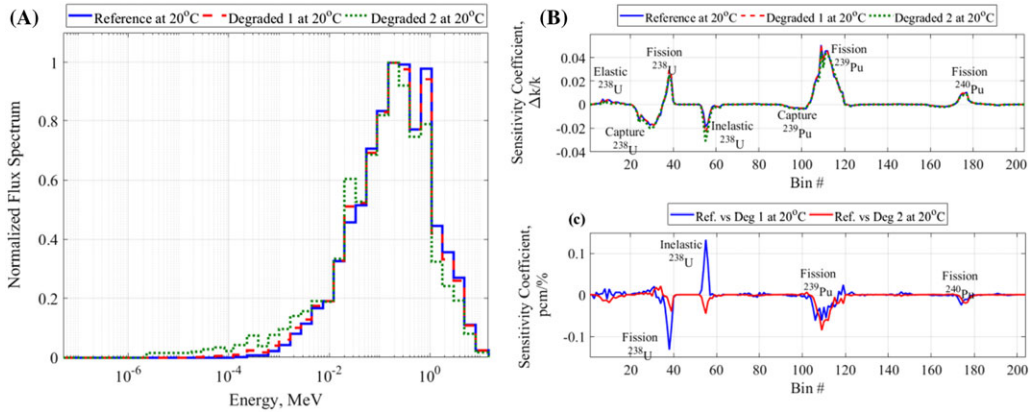

FIGURE 12 Comparison of different parameters for all configuration at 20°C. A, Normalized flux spectrum. B, Sensitivity vector for k_{eff}. C, Sensitivity vector for $\Delta\rho$ [Colour figure can be viewed at wileyonlinelibrary.com]

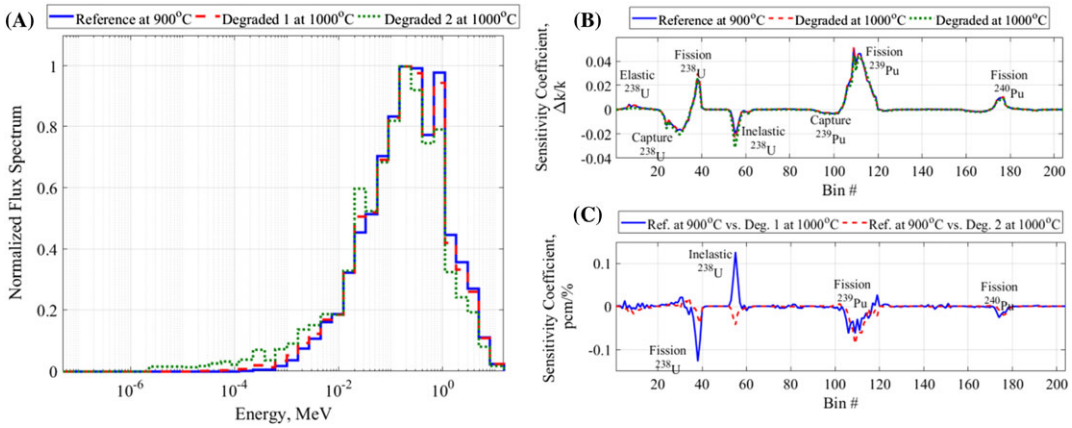

FIGURE 13 Comparison of different parameters for all configurations at 900°C. A, Normalized flux spectrum. B, Sensitivity vector for k_{eff}. C, Sensitivity vector for $\Delta\rho$ [Colour figure can be viewed at wileyonlinelibrary.com]

The temperature impact is shown on all the parameters (flux and sensitivity vectors). The temperature rise reduces the values of all the parameters in the fast energy domain and slightly increases them in the intermediate range (visible for ^{238}U). A similar effect is observed when examining the propagated uncertainties (Figure 14 with COMAC-V01 and Figure 15 with UCOM-V01AB), ie, as the temperature rises, the propagated uncertainties decrease. Furthermore, the same effect of uncertainty reduction is visible when switching between the different variance-covariance matrices. However, in this case, the changes do not affect significantly the isotopic/reaction contribution, which is not the case for the propagated uncertainties on multiplication factor (Figure 8).

Thus, all the information required for the representativity process has been presented. The next 2 sections deal with the search of the ZEPHYR most representative configuration, based on the multiplication factor for the reference case and the reactivity variation for configuration pairs.

4.3 | Reference configuration multiplication factor representativity

As mentioned previously, the first step of the representativity process is to identify the most representative configuration for the reference configuration in ASTRID to be loaded in ZEPHYR. This configuration is to serve as sort of anchor for all the other reactivity variation representativity and is discussed in Section 4.4. It should be noted that, while not presented in this study, successful attempts were made to find 2 representative ASTRID configurations (reference and degraded) with the multiplication factor being the examined parameter. However, those 2 highly representative cases of the multiplication factor do not ensure good representativity of reactivity variation between the ASTRID and the ZEPHYR systems.

The governing assumptions for this and the following part is that the fuel is similar in the 2-fissile zone and the length proportions of the different zones of the ASTRID

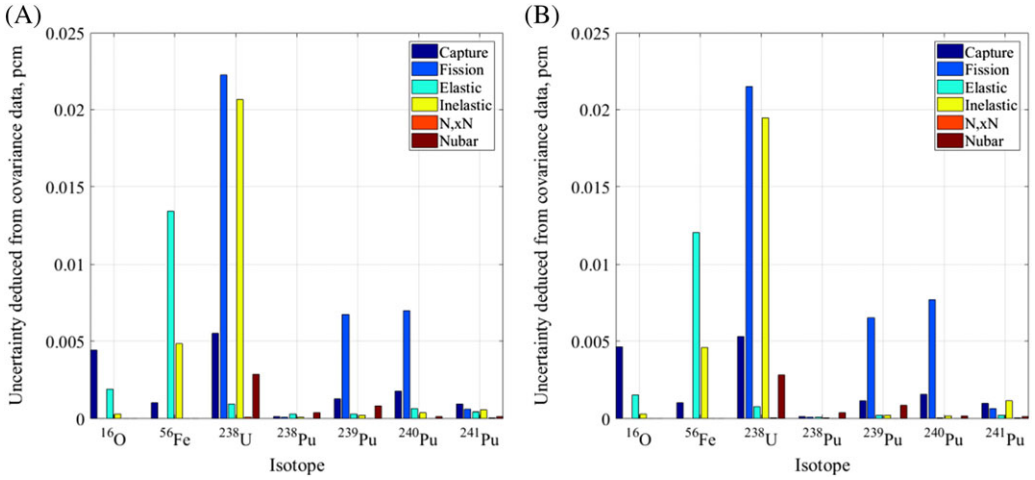

FIGURE 14 Propagated uncertainties isotope/reaction break down for reactivity variation between Reference and Degraded 1 configurations with COMAC-V01. A, 20°C. B, 900°C [Colour figure can be viewed at wileyonlinelibrary.com]

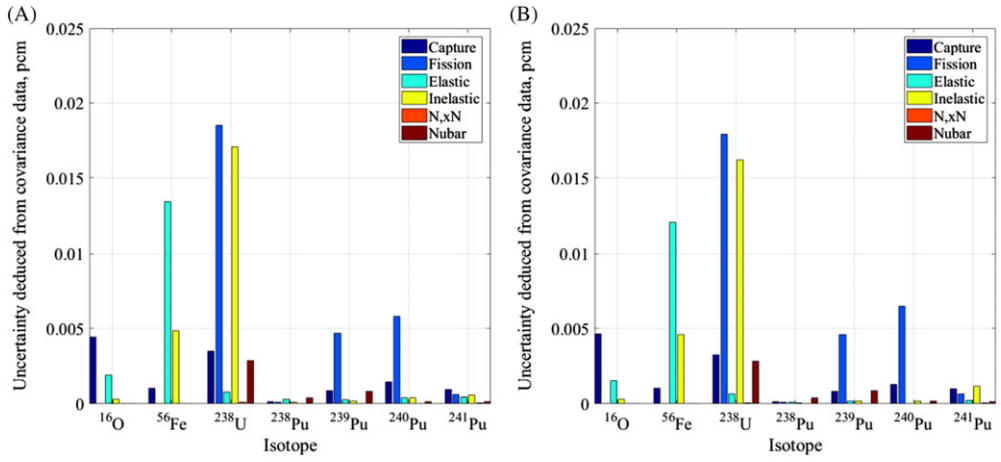

FIGURE 15 Propagated uncertainties isotope/reaction breakdown for reactivity variation between Reference and Degraded 1 configurations with UCOM-V01AB. A, 20°C. B, 900°C [Colour figure can be viewed at wileyonlinelibrary.com]

fuel assemblies are conserved in the ZEPHYR configuration. Thus, the PSO optimization is performed on the content of the PuO_2 in the MOX fuel located in the different zones of the fuel assemblies, while, as stated previously, the Pu vector is regarded as a constant. The geometry of the reference case is presented in Figure 16. As can be seen from the 2-reference configuration of ASTRID (Figure 7A) and the ZEPHYR (Figure 16), there are notable height differences. The ASTRID assembly (without the top voided area) makes in total a 110 cm, while the ZEPHYR assembly makes about 90 cm in total height. This creates the main challenge for the current study since the 20-cm difference is equal to about 2 mean free paths of the neutron in a fast spectrum system (approximately 10 cm[30]), which could potentially lead to enhancement of leakage and decreased scattering effects. Therefore, adjustment of the plutonium in the 2 fissile zones should be done in a manner that would compensate those 2 effects.

The optimization results for the reference configuration zone are summarized in Figure 17 and in Table 6. The results presented in Figure 17 contain all the known positions of all the particles in the swarm. This kind of representation allows examining possible tendencies in the problem behavior. The reference configuration representativity process shows a clear parabolic tendency around a single maximum (which is shown in Table 6) for all the cases.

As can be seen from the results in Table 6, the temperature effects that lower the multiplication factor in the ASTRID core (Table 4) are transferred into density effects in such way that the multiplication factor decreases in the ZEPHYR as well. The uncertainties behavior for the 2 ZEPHYR configuration, shown in Figure 18, is very

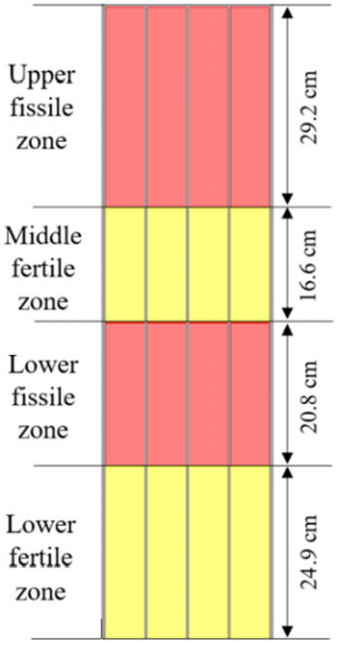

FIGURE 16 ZEPHYR reference fuel assembly [Colour figure can be viewed at wileyonlinelibrary.com]

similar to the uncertainties for the ASTRID configuration with fuel at different temperatures (Figure 8), and the representativity is driven by the high uncertainty of ^{238}U and ^{239}Pu.

In addition to the representativity results obtained using the COMAC-V01 matrix, the same representativity process of the 900°C ASTRID fuel assembly is performed with the updated UCOM-V01AB matrix

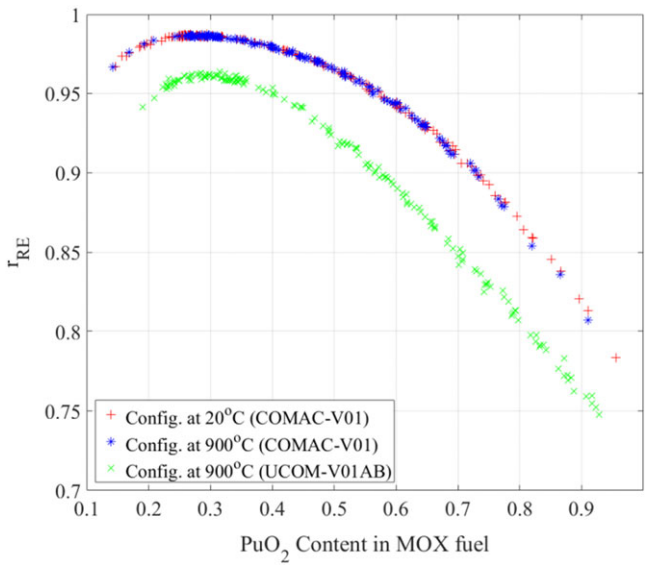

FIGURE 17 Particle swarm optimization results for the plutonium content of the reference configuration [Colour figure can be viewed at wileyonlinelibrary.com]

(presented in Section 2.3). The PSO results of this simulation are marked in green in Figure 17. It is noticeable that the maximum representativity drops from approximately 0.99 to approximately 0.96 and requires more PuO_2 in the fissile zone. Although the decrease is about 3% in the representativity factor, the 2 results are satisfactory.

To understand the differences shown in Figure 17, one should examine the material balance and the driving uncertainties in this case. The plutonium vector suggested for the ZEPHYR is presented in Table 7, and this vector is based on the available MOX pins from the MASURCA stockpile. The impact of UCOM-V01AB on the propagated uncertainties is to significantly reduce the propagated uncertainties from ^{238}U and ^{239}Pu, leading to the increase in the relative importance of the ^{240}Pu isotope. Therefore, due to the substantial differences in the quantities of the ^{240}Pu isotope in the 2 assemblies (Tables 2 and 7 of ASTRID and ZEPHYR, respectively), it is required to find a trade-off between reduction of ND uncertainties and the impacts of each plutonium isotope on the representativity, which cannot be made without loading the same plutonium vector into the ZEPHYR. This leads to the lower representativity factor in comparison to the previous result obtained with COMAC-V01. The trade-off between the highest r_{RE} and plutonium content could be seen from the breakdown of uncertainties for the ASTRID assembly (Figure 11B) and the ZEPHYR (Figure 19), where the differences are clearly seen in the propagated uncertainty of fission in ^{240}Pu.

Three reference ZEPHYR assemblies were obtained during this stage, which exhibits high r_{RE} values. However, when the ND uncertainties are reduced, the representativity factors drop, as the differences in the material content in the 2 cores start to play a larger part in the entire process. This leads to the question whether it is possible to achieve the same high representative experimental configurations with (artificially) reduced ND uncertainties relaying on the process presented in Equation 1? The sensitivity of Equation 1 to reduction in the ND uncertainties could potentially lead to a situation, where high values of r_{RE} could not be achieved due to differences in the material balance of the 2 cores.

4.4 | Reference configuration reactivity variation representativity

As previously, the geometrical proportionality assumption holds for the representativity calculations of the assembly reactivity effect. The relative heights of the degraded ASTRID configurations (Figure 7B,C) are conserved, to

TABLE 6 Particle swarm optimization results for the reference configuration search

Configuration	Matrix Version	r_{RE}	PuO_2 Content in MOX, %	Multiplication Factor
Ref. at 20°C	COMAC-V01	0.988	29.35	1.39777 ± 1.8E-04
Ref. at 900°C	COMAC-V01	0.987	28.61	1.37952 ± 1:8E-04
Ref. at 900°C	UCOM-V01AB	0.964	31.48	1.44828 ± 1:7E-04

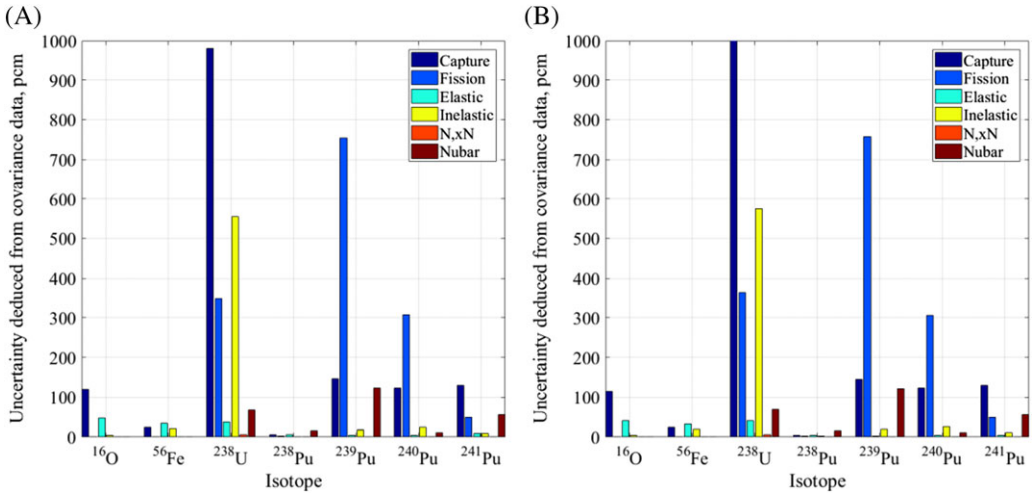

FIGURE 18 Reaction-isotope propagated uncertainty breakdown for 2 reference configurations with COMAC-V01 for ZEPHYR assembly. A, Config. at 20°C. B, Config. at 900°C [Colour figure can be viewed at wileyonlinelibrary.com]

TABLE 7 Approximate plutonium vector of the ZEPHYR assembly

^{238}Pu	^{239}Pu	^{240}Pu	^{241}Pu	^{242}Pu	^{241}Am
0.8%	70%	18%	8%	2%	0.2%

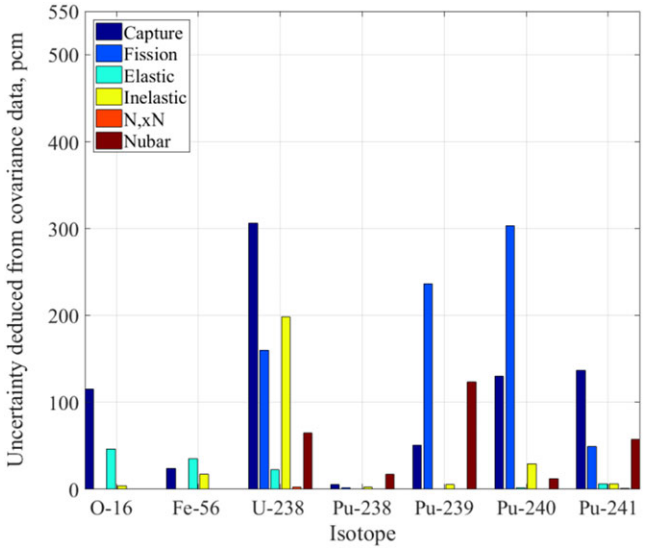

FIGURE 19 Reaction-isotope propagated uncertainty breakdown for 900°C reference configuration with UCOM-V01AB for ZEPHYR assembly [Colour figure can be viewed at wileyonlinelibrary.com]

simplify the search space. The ZEPHYR degraded configurations are shown in Figure 20, where the PSO in each degraded case is executed on the plutonium oxide content in each fissile zone. Thus, the 2-zone configuration (Figure 20A) induces a 2-dimensional search, respectively, whereas the single fissile zone configuration (Figure 20B) corresponds to a 1-dimensional search.

The 2-dimensional results are summarized in Figure 21. The results exhibit the same type of behavior in all the different cases. The results are divided into 3 zones. The first region corresponds to the high plutonium content with representativity factor around 0.6 to 0.7, the second region corresponds to representativity factor equals to zero (ie, "Death Valley"), and the third region of high representativity factors around 0.85, which corresponds to the target value. The 3 zones' behavior is non-trivial and could be explained by examining the reactivity variation sensitivity vector. In the first zone, where the content of the plutonium is high, the relation between the sensitivity vector and the reactivity variation is such that the representativity factor is quite constant. The second zone, where the representativity factor is close to zero, is, in fact, misleading since the r_{RE} values are actually negative. In this case, the sensitivity vector of ASTRID and ZEPHYR have similar behavior but with opposite sign, which results in a negative value of

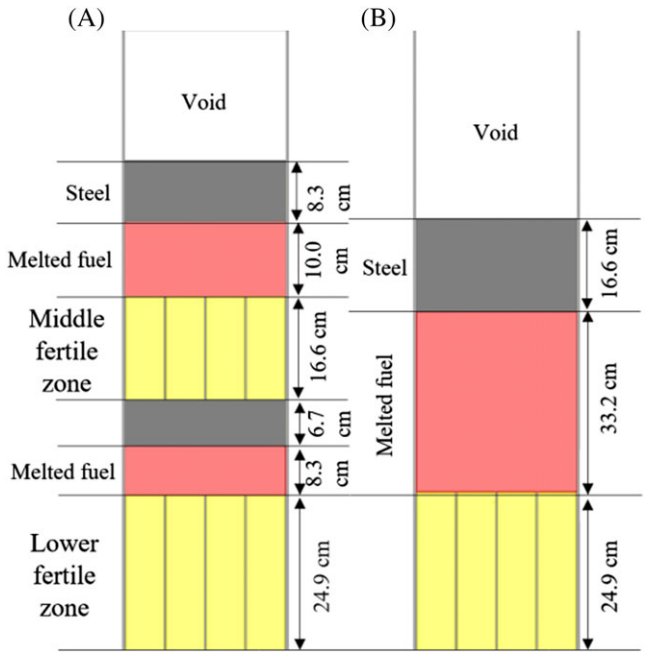

FIGURE 20 ZEPHYR representative configuration under investigation in the representativity process. A, Degraded configuration 1. B, Degraded configuration 2 [Colour figure can be viewed at wileyonlinelibrary.com]

r_{RE} (up to −1). In the PSO sequence, these particles are penalized, by assuming a value of zero.

The results show that for all high fuel temperature cases (Figure 21B-D), acceptable solutions can be found in the range of plutonium content of 20% to 24% in each of the areas. However, there is a notable difference in the behavior when the reference configuration and the degraded configuration fuel remain in 20°C (Figure 21A).

The difference between a system at 20°C and at 900°C clearly demonstrates the impact of the Doppler (fuel temperature) effect on the representativity process. The reference configuration multiplication factor for the most representative configurations at 20°C is about 2000 pcm higher than that at 900°C, as shown in Table 6. This results from the larger amount of PuO_2 content in 20°C, which is required to achieve representativity. The initial high content of PuO_2 in the 20°C system requires a higher PuO_2 content in the degrade configuration (in comparison to the 900°C-1000°C configurations), to achieve the desired representativity factor of 0.85. Accordingly, Figure 21 shows that to achieve high values of r_{RE}, the PSO particles shift towards the acceptance region of 30% to 35%.

The 1-dimensional search results are summarized in Figure 22. The results show that on the contrary to the 2-dimensional search, there is only a single value for the plutonium content that ensures an acceptable r_{RE} value. Furthermore, in this case, the effect of the temperature variation between the reference and the degraded configuration of the ASTRID is visible from the material balance in the degraded configuration of the ZEPHYR, as shown in Table 8. However, this change remains limited as the associated reactivity variation is large (resulting from the problem definition, ie, radial reflective boundary conditions).

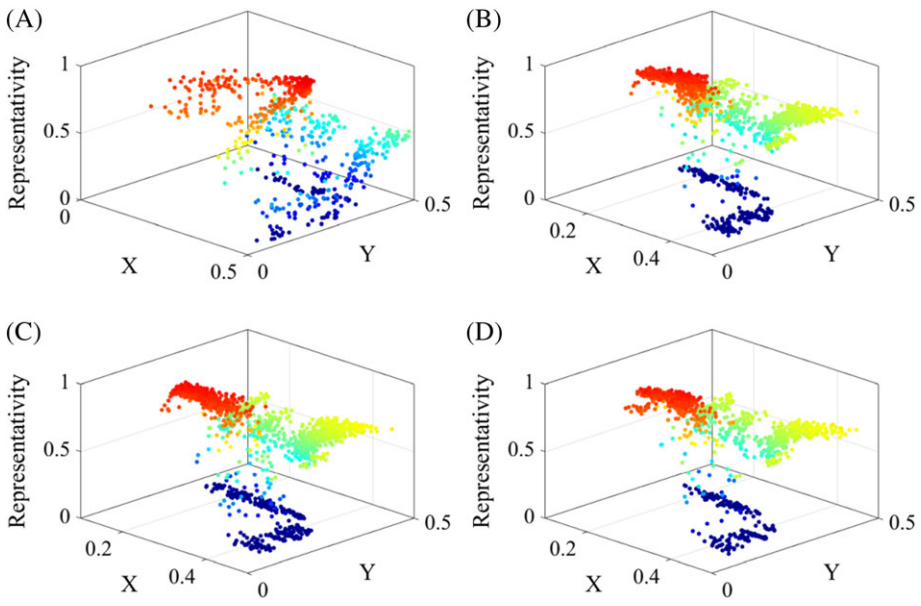

FIGURE 21 Results of the particle swarm optimization for the reactivity variation representativity between reference configuration (Figure 16) and degraded 1 configuration (Figure 20A), where X represents PuO_2 content in zone 1 and Y in zone 2. A, 20°C. B, 1000°C. C, 2000°C. D, 3000°C [Colour figure can be viewed at wileyonlinelibrary.com]

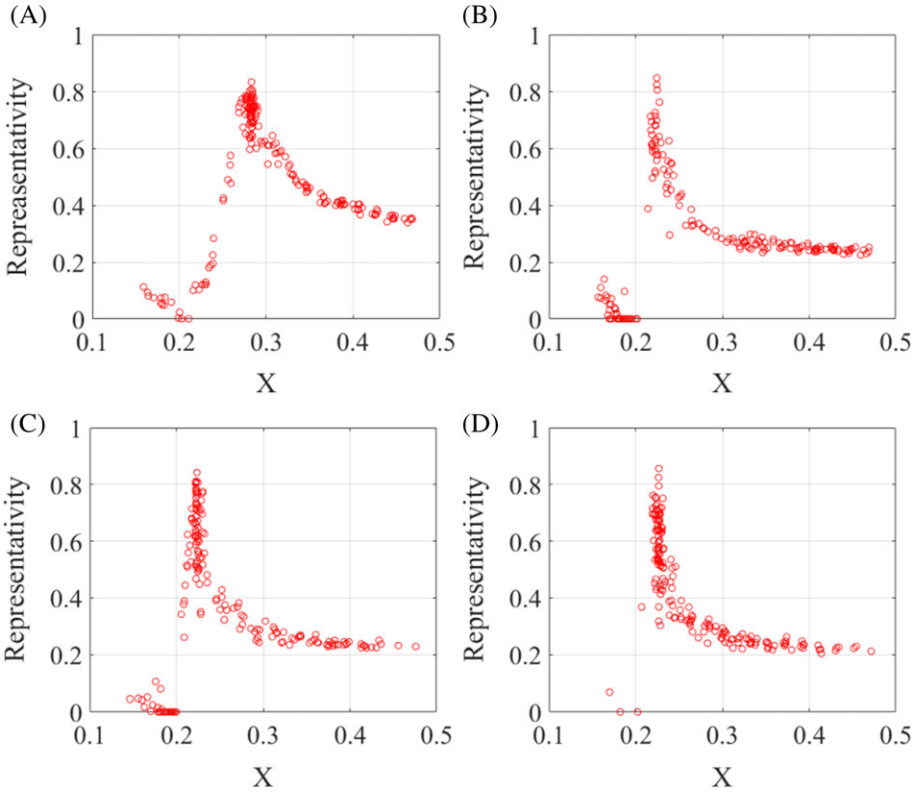

FIGURE 22 Results of the particle swarm optimization for the reactivity variation representativity between reference configuration (Figure 16) and degraded 1 configuration (Figure 20B), where X represents PuO_2 content in the degraded zone. A, 20°C. B, 1000°C. C, 2000°C. D, 3000°C [Colour figure can be viewed at wileyonlinelibrary.com]

TABLE 8 Approximate plutonium content of the ZEPHYR core using COMAC-V01AB

Configure/Temperature	PuO_2 Content		r_{RE} Value
Configuration 1	**Zone 1**	**Zone 2**	
20°C	30%-35%	30%-35%	0.85-0.91
1000°C	20%-24%	20%-24%	0.85-0.87
2000°C	20%-24%	20%-24%	0.85-0.87
3000°C	20%-24%	20%-24%	0.85-0.87
Configuration 2			
20°C	28.3%	...	0.84
1000°C	22.5%	...	0.85
2000°C	22.3%	...	0.85
3000°C	22.2%	...	0.85

The behavior of the result changes in comparison to the 2-dimensional results. As the plutonium content increases, the representativity factor is reduced, and converge to r_{RE} values of about 0.2 to 0.3. As the plutonium content decreases, there is an increase in the r_{RE} value, until it reaches a global maximal point. The reduction of the plutonium content reveals the presence of the Death Valley on the opposite side of the maximal point, in comparison to the 2-dimensional results. The Death Valley is followed by a slight increase of the r_{RE} values. Thus, the 3-zone structure appears also for a single zone optimization.

The results for all the degraded configurations are summarized in Table 8. The preliminary study shows that there are various possible representative configurations for the examined degraded cases, whereas the Doppler Effect from the ASTRID configuration is visible only for a single zone optimization, as can be seen in Table 8 for configuration 2 with the decreasing values of the PuO_2 content. The propagated uncertainties through the COMAC-V01 version (Figure 23) exhibit the same behavior as the $\Delta\rho$ propagated uncertainties in the ASTRID environment (Figure 14). Although the sensitivity vectors between the reactivity variation in the ASTRID (Figures 12 and 13) and the ZEPHYR are different, a close examination of areas with the highest uncertainties in ND in COMAC (eg, in energy range between 100 keV and 1 MeV) reveals some similarity between them.

Finally, the impact of the covariance matrix with reduced uncertainties (UCOM-V01AB) on the representativity of the reactivity variation in the clear configuration is examined. The study is performed on 2 degraded configurations with reference fuel temperature changing from 900°C to 1000°C. The results are summarized in

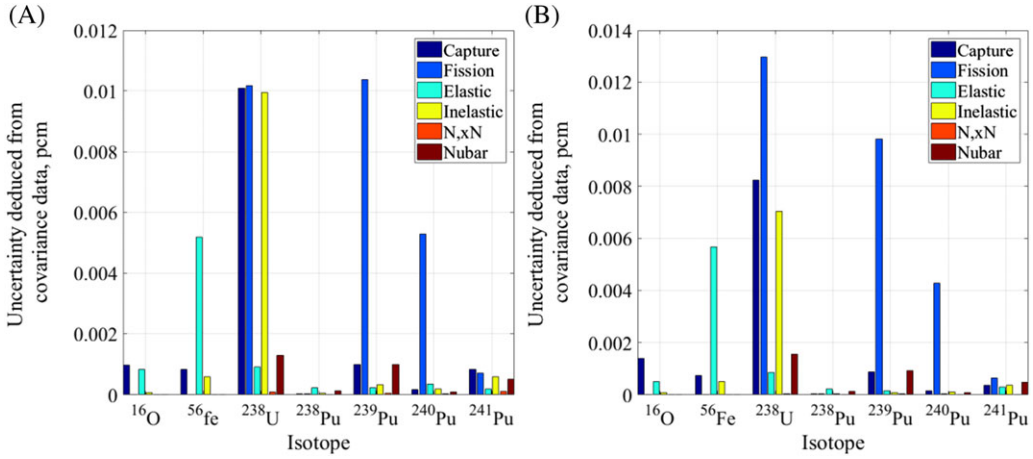

FIGURE 23 Propagated uncertainties isotope/reaction breakdown for reactivity variation between Reference and Degraded 1 of the ZEPHYR configurations with COMAC-V01. A, Fuel at 20°C. B, Fuel at 1000°C [Colour figure can be viewed at wileyonlinelibrary.com]

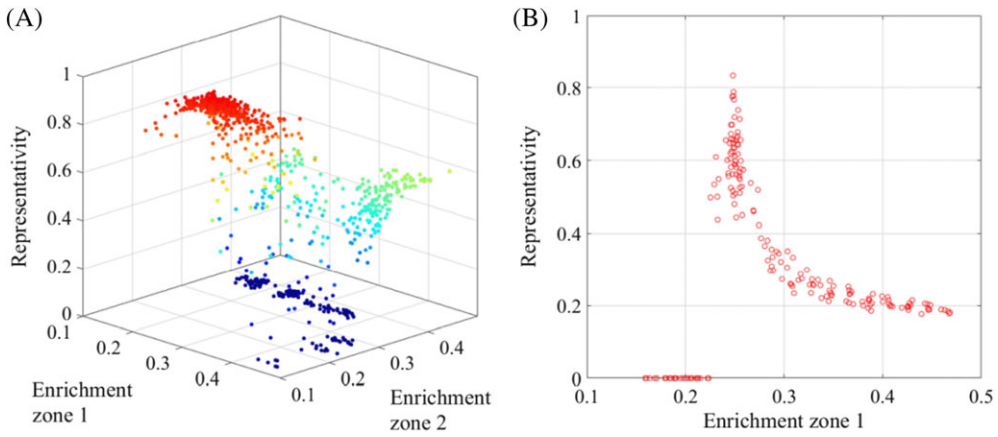

FIGURE 24 Representativity results of the 2-degraded situation using UCOM-V01AB. A, Fuel at 1000°C two zones. B, Fuel at 1000°C single zone [Colour figure can be viewed at wileyonlinelibrary.com]

Figure 24 and in Table 9. The results exhibit similar tendencies to the COMAC-V01 results, ie, a larger Pu content due to low ^{240}Pu content in the ZEPHYR. In the 2 cases, an increase in the plutonium content is clearly seen (Table 8 vs Table 9).

In the case of the 2-zone optimization, a zone where the results obtained from the 2 different matrices have a crossover is visible, from 22.5% to 24% enrichment in the 2 fissile zones. For the single zone optimization, an increase in the plutonium content is present to compensate the low ^{240}Pu content in the 2 cores.

TABLE 9 Approximate plutonium content of the ZEPHYR core using UCOM-V01AB

Configure/ Temperature Configuration 1	PuO_2 Content		r_{RE} Value
	Zone 1	Zone 2	
1000°C	22.5%-26.5%	22.5%-26.5%	0.85-0.91
Configuration 2			
1000°C	25.2%	...	0.85

5 | SUMMARY AND CONCLUSIONS

The present work summarizes the first results of a representativity study dedicated to innovative experimental severe accident neutronics design studies in the future ZEPHYR ZPR. An innovative heuristic approach is implemented, which is based on the coupled use of Monte Carlo perturbation and sensitivity calculations with advanced stochastic optimization method. The results presented in this paper deal with representativity of void and fuel degradation reactivity effects on an assembly design level.

This study is focused on the single fuel assembly behavior, with an emphasis on the temperature treatment, to reach a better representativity of a SCA occurring at high temperature, in a zero-power facility, operating at 20°C. To reach high representativity goal, an optimization process based on the PSO, which uses Serpent 2 Monte Carlo code with sensitivity calculation capabilities, is implemented.[18]

This paper presents a modified PSO algorithm, where a special feature is implemented in the classical PSO (Algorithm 1) to ensure a better local search of each member of the swarm. This is achieved by applying adaptive calculation of the personal and social coefficients. This adaptive algorithm modifies the Serpent input file, executes a sensitivity run, and calculates the representativity factor. The optimization process can target different parameters (either geometry or material balance).

The optimization process of the representativity factor is applied to 2 hypothetical SCA scenarios in the French sodium fast reactor ASTRID core, both initiated by a total instantaneous channel blockage. Therefore, the reference configuration, from which the reactivity variation is calculated, corresponds to an intact but voided SFR fuel assembly. The reference configuration is considered at 2 fuel temperatures, 20°C and 900°C, where the degraded configurations are examined at 20°C, 1000°C, 2000°C, and 3000°C.

This work focuses on the reactivity variation in the core degradation process; hence, the optimization process implemented here is a 2-step process. The first step is to identify the representative reference configuration, whereas the second step considers the first step's results as a sort of anchor to find the most representative degraded configuration. A simplifying assumption is made within the optimization process, ie, the relative heights of the different zones in the SFR configuration are conserved in the representative ZEPHYR configuration. Thus, the search is performed by changing the material content (plutonium content in the MOX fuel) of each of the fissile zones. Furthermore, the minimal accepted representativity factor is set of 0.85, as there are significant differences between the ZEPHYR and the SFR fuels.

The sensitivity of the representativity calculation is examined against 2 different covariance data matrices (COMAC-V01 and UCOM-V01AB). The COMAC-V01 contains rather high uncertainties on several key isotopes, as presented in the paper, while UCOM-V01AB is updated by using older experimental data available from SNEAK-12A/B severe accident studies experimental program.[15,16,22,23,31] UCOM-V01AB was created for the sole purpose of this project to studying the sensitivity of the optimization process to the changes in the ND uncertainties. It should be noted that COMAC considering some data assimilation from SFR representative configurations, thus consequently, these data are also available in UCOM.

The first stage results show that the representativity factor for the multiplication factor r_{RE} of the SFR fuel assembly is transferred well into the ZEPHYR configuration with r_{RE} above 0.98. The temperature effect is manifested in the PuO_2 content in the MOX fuel, with less plutonium required for the higher temperature (the multiplication factor in the SFR is reduced with the temperature rise). The impact of different covariance data leads to modifications of the representativity factor: By reducing the uncertainties of the driving isotopes (^{238}U and ^{239}Pu), the focus shifts to the third isotope in line, ^{240}Pu, which has a noticeable difference between the 2 fuels (ASTRID—Table 2 vs ZEPHYR—Table 7). This effect is quite small at this stage; however, one should consider the effect of very low uncertainties on the representativity process.

The second stage results are presented for 2 different reactivity variations: 2 melted zones and a single compacted zone. The former is characterized by a 2-dimensional search space on the PuO_2 content in the fuel of the 2 zones. The results (Figure 21) show an interesting behavior of the optimization process. All the results for all the different temperature variations are divided into 3 zones. For high enrichment contents, the representativity factor converged to a constant value. The second zone, the so-called Death Valley (r_{RE} equal to zero), the results exhibit an interesting combination of reactivity variation versus sensitivity profile, which actually lead to negative values of r_{RE}. Finally, the third zone includes the positive representativity factors and the acceptance area of values exceeding 0.85. The impact of the temperature on the results is not visible due to the fact that reduction in the PuO_2 content in one region could be compensated by increase of the PuO_2 content in the other, and vice versa, to reach the same target value. Thus, all the results converge to a similar enrichment zone, as seen in Table 8.

The second part of the optimization process is made on the single compacted zone. In this case, the results (Figure 2) exhibit the same 3-zone search space. However, the effect of the temperature is visible, as shown in Table 8. The results show that there is exactly one single possible solution to achieve r_{RE} of above 0.85.

Finally, for the 2 degraded configurations, the impact of the different covariance matrices is examined. The results show similar tendencies with a higher required PuO_2 content for the modified covariance matrix. However, the results reach the desired representativity factor of 0.85.

This paper summarizes the first attempt to study the neutronic behavior of severe accident, which paves the way to establishing supporting experimental programs in the ZEPHYR facility. The paper presents studies on possible accidental scenarios in the ASTRID core, with their transfer through the representativity scheme into the ZEPHYR environment. The main focus is put on the impact of the temperature on the SCA in the ASTRID, and how these temperature effects can be transferred into density effects in a zero-power facility. As shown in the paper, such configuration can be found through an optimization process, for the different stages with different conditions. One should bear in mind that satisfactory representativity at the assembly level does not guarantee satisfactory representativity of full core effects. The assembly level studies are indispensable since they serve as a proof-of-concept. They are here considered as a starting point for studying full core representative configurations and for examining the impact of different physical parameters on the representativity process, which is the next part of this study. This methodology will be used to study full SFR and ZEPHYR core representative configurations.

ACKNOWLEDGEMENTS

This R&D work was performed within a scientific collaboration program between CEA Cadarache and Ben-Gurion University of the Negev.

The research was partially funded by the Israeli Ministry of Energy, contract number 215-11-020.

ORCID

M. Margulis http://orcid.org/0000-0002-7188-3301
P. Blaise http://orcid.org/0000-0003-4609-5351
E. Gilad http://orcid.org/0000-0002-2130-9301

REFERENCES

1. Kasahara N. *Fast Reactor System Design*. Singapore: Springer; 2017.
2. Gomez A, Azzaro-Pantel C, Domenech S, et al. Exergy analysis for Generation IV nuclear plant optimization. *International Journal of Energy Research*. 2009;34(7):609-625.
3. Hartanto D, Kim C, Kim Y. A comparative physics study for an innovative sodium-cooled fast reactor (iSFR). *International Journal of Energy Research*. 2016; Published online in Wiley Online Library;1-12.
4. Sehgal BR. *Nuclear Safety in Light Water Reactors*. Amsterdam: Elsevier; 2012.
5. Dos Santos N, Blaise P, Santamarina A. A global approach of the representativity concept: application on a high-conversion sub-moderated MOX lattice case. Paper presented at: M&C-2013, 2013; Sun Valley, ID, USA.
6. Dos Santos N, Blaise P, Santamarina A. Impact of mock-up experimental correlations and uncertainties in the transposition process. Paper presented at: ANIMA-2013, 2013; Ghent, Belgium.
7. Lebrat JF, Tommasi J. The use of representativity theory in the depletion calculations of SFR blankets. *Annals of Nuclear Energy*. 2017;101:429-433.
8. Bertrand F, Marie N, Prulhiere G, Lecerf J, Seiler JM. Comparison of the behavior of two core designs for ASTRID in case of severe accidents. *Nuclear Engineering and Design*. 2016;297:327-342.
9. Blaise P, Boussard F, Leconte P, et al. Experimental R&D innovation for Gen-II, III & IV neutronics studies in ZPRs: a path to the future ZEPHYR facility in Cadarache. Paper presented at: IGORR-2016, 2016; Berlin, Germany.
10. Zhang Q, Mclellan BC. Review of Japan's power generation scenarios in light of the Fukushima nuclear accident. *International Journal of Energy Research*. 2014;38(5):539-550.
11. Ros P, Leconte P, Blaise P. Re-Interpretation of the ERMINE-V experiment validation of fission product integral cross-section in the fast energy range potential for recriticality of the relocated core. Paper presented at: Nuclear Data ND2016, 2016; Brugge, Belgium.
12. Ros P, Leconte P, Blaise P, Dofer de Soebille H, Maillot M. Fast-thermal coupled cores in zero power reactors: a demonstration of feasibility and pertinence for the ZEPHYR project. *Annals of Nuclear Energy*. 2017;110:290-305.
13. Orlov VV. Problem of fast reactor physics related to breeding. *Atomic energy review*. 1980;January:;989-1077.
14. Ronen Y. *Uncertainty Analysis*. Boca Raton, Florida: CRC Press; 1988.
15. Margulis M, Blaise P, Mellier F, Gilad E. The path for innovative severe accident neutronics studies in ZPRs. Part I.2—impact of nuclear data uncertainties on reactivity changes of SNEAK-12A core. *Progress in Nuclear Energy*. 2017;96:97-117.
16. Margulis M, Blaise P, Millier F, Gilad E. The path for innovative severe accident neutronics studies in ZPRs. Part II.2 - Impact of nuclear data uncertainties on reactivity changes of SNEAK-12B core. Progress of Nuclear Energy; Submitted for review.
17. Kennedy J, Shi Y, Eberhart RC. *Swarm Intelligence*. San Francisco, CA: Morgan Kaufmann; 2001.
18. Aufiero M, Bidaud AV, Hursin M, et al. A collision history-based approach to sensitivity/perturbation calculations in the continues energy Monte Carlo code Serpent. *Annals of Nuclear Energy*. 2015;85:245-258.
19. Chaturvedi KT, Pandit M, Srivastava L. Particle swarm optimization with time varying acceleration coefficients for non-convex economic power dispatch. *Electrical Power and Energy Systems*. 2009;31:249-257.
20. De Saint Jean C, Archier P, Noguere G, et al. Estimation of multi-group cross sections covariances. Paper presented at: PHYSOR-2012, 2012; Knoxville, Ten, USA.

21. Koning AJ, Bauge E, De Saint Jean C, et al. Status of the JEFF Nuclear Data Library. *Journal of the Korean Physics Society.* 2011;59(2):1057-1062.
22. Margulis M, Blaise P, Gabrielli F, Gruel A, Mellier F, Gilad E. The path for innovative severe accident neutronics studies in ZPRs. Part I.1—analysis of SNEAK-12A experiments for core disruption in LMFBRs. *Progress in Nuclear Energy.* 2017;94:106-125.
23. Margulis M, Blaise P, Gabrielli F, Gruel A, Mellier F, Gilad E. The path for innovative severe accident neutronics studies in ZPRs. Part II.1 - Analysis of SNEAK-12B experiments for core disruption in LMFBRs. Progress in Nuclear Energy; Submitted for review.
24. Generation IV International Forum. A technology roadmap for Generation IV nuclear energy systems 2002.
25. Chenaud MS, Devictor N, Mignot G, et al. Status of the ASTRID core at the end of the pre-conceptual design phase 1. *Nuclear Engineering and Technology.* 2013;45(6):721-730.
26. Gabrielli F, Rineiski A, Vezzoni B, Maschek W, Fazio C, Salvatores M. ASTRID-like fast reactor cores for burning plutonium and minor actinides. *Energy Procida.* 2015;71:130-139.
27. Krivitchik G, Blaise P, Coquelet-Pascal C. Artificial neural network surrogate development of equivalence models for nuclear data uncertainty propagation in scenario studies. *EPJ Nuclear Science and Technology.* 2017;3(22):1-15.
28. Ruggieri JM, Tommasi J, Lebart JF, et al. ERANOS 2.1: international code system for GEN IV fast reactor analysis. Paper presented at: ICAPP 2006, 2006; Reno, NV, USA.
29. Tommasi J, Archier P, Rimpault G. Sodium void validation with ERANOS on zero power facility experiments. Paper presented at: PHYSOR-2016, 2010; Pittsburg, PA, USA.
30. Yang WS. Fast reactor physics and computation methods. *Nuclear Engineering and Technology.* 2012;442(2):177-198.
31. Margulis M, Blaise P, Rimpault G, Gilad E. Interpretation of the SNEAK-12A/B experimental programs on severe core accidents in LMFBRs—some feedback on nuclear data re-assimilation for the prediction of reactivity changes. Paper presented at: ICAPP-2017, 2017; Fukui/Kyoto, Japan.

How to cite this article: Margulis M, Blaise P, Gilad E. Modeling representative Gen-IV molten fuel reactivity effects in the ZEPHYR fast/thermal coupled ZPRs. Part I—Assembly level. *Int J Energy Res*. 2018;42:1950–1972. https://doi.org/10.1002/er.3991

APPENDIX A

PARTICLE SWARM OPTIMIZATION: GENERAL OVERVIEW AND TERMINOLOGY

Particle swarm optimization (PSO) is a population-based stochastic optimization technique[17] inspired by *social* behaviors of birds or fish, for example. Particle swarm optimization shares many similarities with evolutionary algorithms such as genetic algorithms (GAs) and bee colonies. The system is initialized with a random population (aka particles), which is evaluated for the first time, and the *position* is determined for the initial population distribution. Unlike the GA that updates the population by crossovers and mutation, the PSO population of particles is updated using the *velocity*, which describes how the particle is "flying" through the problem's search space. Compared to GA, the advantages of PSO are that PSO is easy to implement and there are few parameters to adjust. A general overview of Algorithm 1 is shown in Figure A1.

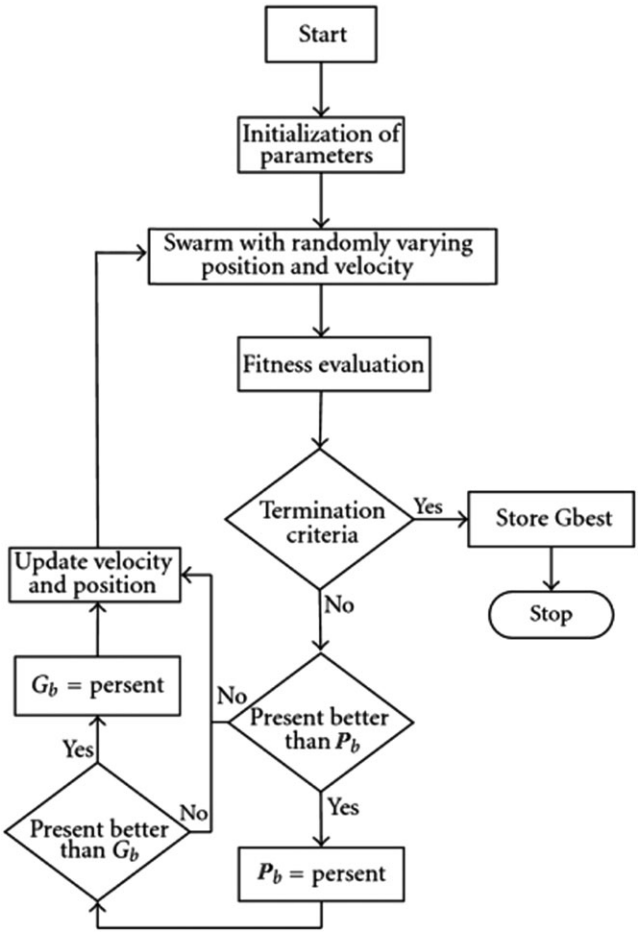

FIGURE A1 A general particle swarm optimization algorithm[17]

Basic terminology definition (alphabetical order):

Cognitive—The memory of a single particle to its best-obtained solution up until the current iteration, c_1 in Equation 3.

Global best—The best estimation of the target function that the entire swarm had until the current iteration.

Inertia—The impact of the previous motion direction of the particle on the subsequent iteration, ω in Equation 3.

Particle—An individual in the optimization process.

Personal best—The best estimation of the target function that a single particle had until the current iteration.

Position—The value of the target function for a given particle.

Social—The memory of the entire swarm to its best-obtained solution up until the current iteration, c_2 in Equation 3.

Velocity—The change rate of the particle's position in the search space according to *cognitive* and *social* factors.